Talanta 268 (2024) 125294

Contents lists available at ScienceDirect

Talanta

journal homepage: www.elsevier.com/locate/talanta

Geldanaycin-encapsulated magnetic nanoparticle for isolation of myosin in proteomics

Qing Chen [a,1], Yan Xu [a,1], Xueting Feng [a], Yuhan Xiang [a], Jiayue Ni [a], Guoyu Ding [a,*], Qunxiang Ren [a,**], Ming-sheng Zhou [b]

[a] School of Pharmacy, Shenyang Medical College, Shenyang, 110034, China
[b] Shenyang Key Laboratory of Vascular Biology, Science and Experiment Center, Shenyang Medical College, Shenyang, 110034, China

ARTICLE INFO

Handling Editor: J. Wang

Keywords:
Magnetic nanoparticle
Geldanamycin
Myosin
Separation and purification of the proteins
Solid phase extraction

ABSTRACT

The grafting of a drug molecule, i.e., geldanamycin (GA) onto polyethyleneimine (PEI)-coated magnetic nanoparticle produces a novel composite, GA@Fe_3O_4–NH_2. The composite is confirmed by characterizations with FT-IR, Raman, SEM, EDS, VSM and TEM. Due to the high binding-affinity of GA with myosin heavy chain (MYH), GA@Fe_3O_4–NH_2 exhibits excellent adsorption performance towards myosin. Consequently, a solid-phase extraction procedure is established for highly efficient and selective separation of myosin from pig heart extract. At pH 6.0, an adsorption efficiency of 97.1 % is achieved for treating 100 μg mL^{-1} myosin (0.1 mL) with 0.1 mg GA@Fe_3O_4–NH_2 as adsorbent. The adsorption behavior of myosin onto GA@Fe_3O_4–NH_2 fits Langmuir model, corresponding to a theoretical adsorption capacity of 518.1 mg g^{-1}. The adsorbed myosin can be readily recycled by the SDS solution (1 %, m/m) with an elution efficiency of 91.8 %. According to circular dichroism spectroscopy, the conformational changes of myosin during adsorption and elution are reversible. For practical application, myosin is successfully isolated from the pig left ventricular protein extract with GA@Fe_3O_4–NH_2, and SDS-PAGE and LC-MS/MS showed that myosin had high purity and a total of 716 proteins could be identified. Significantly, Geldamycin-encapsulated magnetic nanoparticle for the separation of myosin well exploits the potential of the nanomaterials modified by drug molecules in the separation and purification of target proteins.

1. Introduction

As the molecular motor of the cytoskeleton, myosin is the main structural protein of the heart muscle, drives muscle contraction by converting chemical energy generated by ATP hydrolysis into mechanical force and plays a key role in muscle regulation, development, and mechanotransduction [1–5]. Studies have shown that changes in the structure or function of myosin are directly related to cardiac diseases such as ventricular dysfunction, heart failure and arrhythmia [6,7]. Therefore, effective isolation and purification of myosin from cardiac tissue is an important prerequisite for in-depth study of the pathogenesis and preventive measures of myocardial disease at the molecular level.

In recent years, the solid-phase extraction (SPE) techniques have promoted the separation and concentration of analytes from liquid samples, or the cleaning of previously processed extracts. Compared with common methods, such as isoelectric precipitation, organic solvent precipitation, dialysis, ultrafiltration, chromatography, electrophoresis, crystallization etc, SPE has the advantages of less solvent usage, simple operation, high selectivity and little interference [8–11]. This can save pretreatment time, improve efficiency, and has prompted the exploration of new adsorbents that can overcome the major drawbacks of traditional protein sample pretreatment by taking advantage of specific interactions with proteins [12–14]. The field of protein separation and purification is to design functional solid phase materials with specialized molecular modifications that can interact with protein domains while preserving the structure and activity of the proteins [15,16].

Magnetic solid phase extraction (MSPE) was developed for enable easy, low cost and rapid SPE processes [17]. Magnetic nanoparticles (MNPs) are a new type of organic-inorganic functional material composed of magnetic materials and polymers. Because of their

* Corresponding author.
** Corresponding author.
E-mail addresses: guoyuding@mail.nankai.edu.cn (G. Ding), renqunxiang@163.com (Q. Ren).
[1] Qing Chen and Yan Xu contributed equally to this work.

https://doi.org/10.1016/j.talanta.2023.125294
Received 8 August 2023; Received in revised form 18 September 2023; Accepted 6 October 2023
Available online 8 October 2023

excellent superparamagnetic and unique physical and chemical characteristics, including good biocompatibility, high dispersion stability, high surface area, and the ability to manipulate with an external magnetic field [8]. MNPs have improved the capacity to capture target compounds from complex matrices. Moreover, coupling MNPs with functionalized molecules is essential to create target recognition and binding sites for the application of purifying and extracting biological macromolecules (such as complex sample cells, viruses, proteins and nucleic acids) [18–20]. For example, Ni-modified magnetic nanoparticles for affinity purification of His-tagged proteins from the complex matrix of the silkworm fat body [21]. Rapid and simultaneous purification of aflatoxin B1, zearalenone and deoxynivalenol has been achieved using their monoclonal antibodies and magnetic nanoparticles, etc. [22].

Current surface functionalization methodologies can design adsorbents with the ability to realize recognition, separation and characterization of proteins. Drug-coated MNPs have the advantages of being stable in biological circulation systems and readily interacting with cells or other biological units. In this regard, the use of drug-MNPs in separation and purification of proteins is inspired by their targeted interaction with protein domains. Geldanamycin (GA) is an amphotericin antibiotic of the benzo quinoline type, produced by Streptomyces hygroscopicus. It is an inhibitor of heat shock protein (Hsp90) and has strong cytotoxicity to tumor cells [23]. GA is an important tool for studying human tumorigenesis, tumor cell proliferation and cell apoptosis [24]. The hydroquinone moiety of geldanamycin can bind to the ATP binding domain and inhibit the mRNA expression of myosin heavy chain [25]. In addition, GA can prevent phosphorylation of the 20 kDa myosin light chain or other proteins [26].

In this paper, geldanamycin-encapsulated magnetic nanoparticles were used to separate and purify myosin from pig heart extract. In methanol at room temperature, geldanamycin (GA) was bound to the surface of polyethyleneimine (PEI)-coated magnetic nanoparticle (Fe_3O_4–NH_2) through hydrogen interactions, yielding GA@Fe_3O_4–NH_2. Due to the strong affinity between GA and myosin heavy chain domain, GA@Fe_3O_4–NH_2 exhibited high adsorption selectivity for myosin (MYO) under the best experimental conditions. In a practical application, myosin was successfully isolated from porcine left ventricular protein extract with GA@Fe_3O_4–NH_2. Therefore, a new method for protein separation and purification using drug-modified magnetic nanomaterials as adsorbent was established.

2. Experimental

2.1. Materials and reagents

Myosin (MYO), bovine serum albumin (BSA), myoglobin (MYB) and cytochrome C (cyt-c) were purchased from Sigma Aldrich (St. Louis, USA); Protein molecular weight marker (Broad, 3597A) is acquired from Takara Biotechnology (Dalian, China); Polythymidine (PEI) was purchased from Shanghai Aladdin Biochemical Technology Co. Ltd. (Shanghai, China); geldanamycin (GA) was purchased from Shanghai Source Leaf Biotechnology Co. Ltd. (Shanghai, China); Sodium acetate, anhydrous ethanol, ethylene glycol, methanol, tris (hydroxymethyl) aminomethane (Tris), sodium-dodecyl sulfate (SDS), boric acid, glacial acetic acid, Coomassie brilliant blue G250, glycine, NaCl, H_3PO_4, NaOH and EDTA are supplied by Sinopharm Chemical Reagent Co. Ltd. (Shanghai, China). Unless otherwise stated, all reagents are analytically pure and have not undergone any pretreatment before use. Deionized water (ddH_2O) of 18 MΩ cm was used throughout all experiments.

2.2. Instrumentation

Fourier infrared (FT-IR) spectra were obtained using an iS10 FT-IR spectrometer (Thermo Nicolet Corporation, USA) with a range of 400–4000 cm^{-1}. The Renishaw inVia Raman spectrometer (Renishaw, UK) was used to obtain Raman spectra. The SEM images of magnetic nanoparticles were recorded on a HITACHI SU8020 scanning electron microscope (Hitachi, Japan), while TEM images were received on a HITACHI H-7650 transmission electron microscope (Hitachi, Japan). The magnetic characterization was characterized by BKT-4500 vibrating sample magnetometer (Beijing Xinke High-tech Testing Technology Co., LTD, China) at room temperature. The surface element composition of magnetic nanoparticles was ascertained by Oxford X-MaxN 50 EDS spectrometer (Oxford, UK). Quantitative detection of proteins using U-3900 UV–vis spectrophotometer (Hitachi, Japan). pH monitoring was carried out using a PB-10 pH Meter (Beijing Sartorius Instruments Co., Ltd., China). The MOS-450 (Bio-Logic, France) automatic transcription spectropolarimeter was used to acquire Circular dichroism (CD) spectrum at 293K. LC/MS mass spectrometer used in this study was equipped with an Easy nLC 1200 chromatographic system at a nanoliter flow rate (Thermo Fisher Scientific, USA) and a Q-Exactive HF-X mass spectrometer (Thermo Fisher Scientific, USA).

2.3. Synthesis of GA@Fe_3O_4–NH_2

Amino-coated Fe_3O_4 magnetic nanoparticles (Fe_3O_4–NH_2) were prepared by solvothermal synthesis method using polyethyleneimine (PEI) as a stabilizing agent. A mixture of 0.135 g of $FeCl_3{\cdot}6H_2O$ and 1.8 g of sodium acetate was dissolved in 20 mL of ethylene glycol. Then 0.5 g of hyperbranched polyethyleneimine (PEI, 25 kDa) were added dropwise under constant stirring at room temperature for 45 min to form a yellow colloid mixture. Transfer 18.0 mL of the mixture to a polytetrafluoroethylene sealed stainless steel autoclave with a capacity of 50 mL. Set the thermostatic oven temperature to 200 °C, put the autoclave in the oven for reaction for 12 h. Afterward, the solution was cooled to room temperature, and the obtained product was separated by magnetic separation method and washed twice with anhydrous ethanol and twice with distilled water. Dry at 60 °C to obtain Fe_3O_4–NH_2 [27].

9.0 mg of geldamycin was dissolved in 27 mL of methanol to obtain an bright yellow solution. 3.0 mg of Fe_3O_4–NH_2 was then added. After ultrasonic homogenization, the mixed suspension was stirred at room temperature for 24 h. After standing for 10 min, the product was collected with a magnet for 1 min, meanwhile the colour of the supernatant turned pale yellow. The obtained geldanamycin-encapsulated magnetite nanoparticles were washed twice with methanol and twice with water. Finally, the black powder of GA@Fe_3O_4–NH_2 was obtained after drying at 60 °C for 12 h.

2.4. Adsorption and elution of protein by GA@Fe_3O_4–NH_2

To investigate the protein adsorption properties of the GA@Fe_3O_4–NH_2 magnetite nanoparticle, myosin (MYO), bovine serum albumin (BSA), myoglobin (MYB) and cytochrome C (cyt-c) were selected as model proteins. 0.1 mg of GA@Fe_3O_4–NH_2 was added to 200 μL centrifuge tubes, mixed with 100 μL 100 μg mL^{-1} protein solution and shaken for 30 min 60 μL of the supernatant was collected and 300 μL of Coomassie Brilliant Blue G250 solution was added to quantify the residual protein concentration in the solution by the absorption peak intensity at 595 nm of the dyed protein solution. Use the standard working curve to calculate the concentration of protein before and after adsorption. The adsorption efficiency of protein in the experiment is calculated from formula (1):

$$E_1 = \frac{C_0 - C_1}{C_0} \times 100\% \quad (1)$$

where E_1 is the protein adsorption efficiency (%); C_0 is the original concentration of protein prepared in the experiment (μg mL^{-1}); C_1 is the concentration of protein in the solution after adsorption (μg mL^{-1}).

The collected GA@Fe_3O_4–NH_2 after magnetic separation was first added to 100 μL of BR buffer (pH 6.0, 0.04 mol L^{-1}) to remove non-

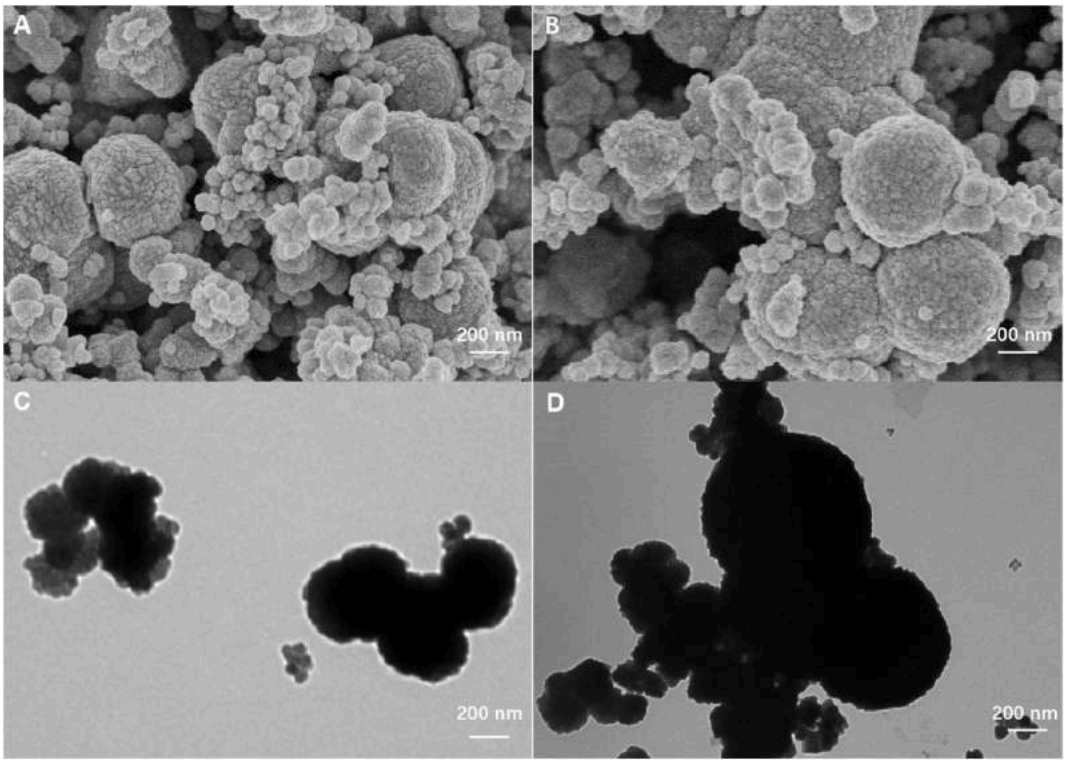

Fig. 1. SEM image of Fe_3O_4–NH_2 (A) and GA@Fe_3O_4–NH_2 (B); TEM image of Fe_3O_4–NH_2 (C) and GA@Fe_3O_4–NH_2 (D).

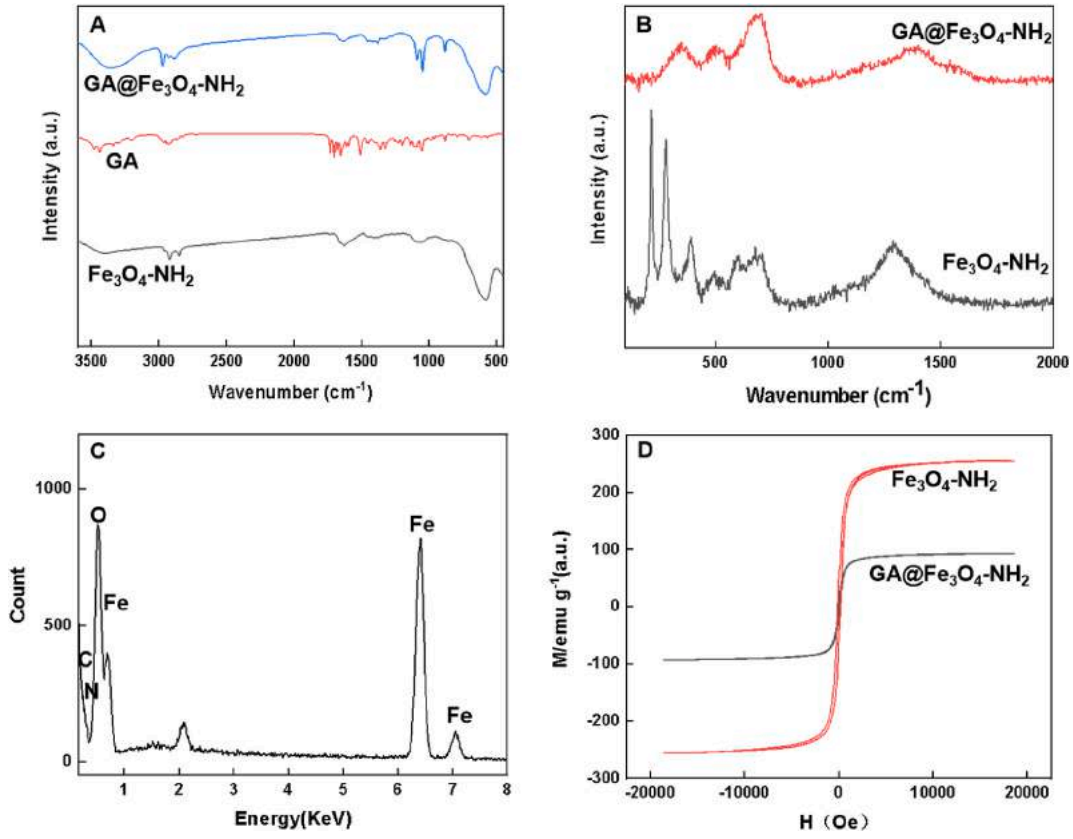

Fig. 2. FT-IR (A) and Raman (B) spectra of Fe_3O_4–NH_2 and GA@Fe_3O_4–NH_2; Energy dispersive X-ray spectrometer (EDS) analysis results for the GA@Fe_3O_4–NH_2 (C); VSM curves of Fe_3O_4–NH_2 and GA@Fe_3O_4–NH_2 (D).

specifically adsorbed proteins. After shaking for 10 min, magnetic separation was performed, and the supernatant was removed. Another 100 μL of 1 % SDS solution was added as an eluent, and the myosin adsorbed on the surface of GA@Fe_3O_4–NH_2 was eluted by shaking for 20 min. Using the magnetic separation method, take the supernatant to determine its absorbance at 595 nm, and calculate the elution efficiency according to the amount of protein in the eluate and the amount of protein adsorbed by the adsorbent. The elution rate of protein in the experiment can be calculated by formula (2).

$$E_2 = \frac{C_2}{C_0 - C_1} \times 100\% \quad (2)$$

Where E_2 is the elution rate of protein, C_0 is the original concentration of protein in the experiment, C_1 is the concentration of white in the solution after adsorption, and C_2 is the concentration of protein in the solution after elution.

2.5. Isolation and identification of myosin from pig heart by GA@Fe_3O_4–NH_2

A certain volume of the crude extract of pig heart protein was taken, diluted 5 times with BR buffer solution (pH 6.0, 0.04 mol L^{-1}), stirred to form a uniform solution, and used as the sample of pig heart protein extract. 0.1 mg of GA@Fe_3O_4–NH_2 was taken and added to 100 μL of the pig heart protein extract sample, shaken for 30 min, and the supernatant was removed. Magnetic separation was achieved by adding 100 μL of BR buffer (pH 6.0, 0.04 mol L^{-1}) and shaking for 10 min, the supernatant was removed, and 100 μL of 1 % SDS solution was added and eluted for 20 min to obtain purified myosin.

3. Results and discussion

3.1. Synthesis and characterization of GA@Fe_3O_4–NH_2

Fe_3O_4–NH_2 were synthesized by a modified procedure via a smooth solvothermal synthetic method, where PEI could be used as an effective protectant to prevent particle aggregation and provide abundant amino groups on the surface of magnetic nanoparticles [28]. In the optimized methanol solution buffer system, a large number of amino groups combine with GA molecules in solution through hydrogen bonding interaction, resulting in GA coating on the surface of magnetic nanoparticles [29–31]. Fig. 1 shows the SEM images and TEM images of Fe_3O_4–NH_2 and GA@Fe_3O_4–NH_2, respectively. It can be seen from Fig. 1 A and C that the synthesized Fe_3O_4–NH_2 is composed by many small particles to form larger spherical particles with particle size of about 500 nm. This is because larger aggregates can be generated by adding high molecular weight polymers [32]. Therefore, the size of the PEI polymer was sufficient to bridge multiple particles together to form large aggregates. Fig. 1B and D shows that the magnetic nanoparticles encapsulated with GA have a relatively flat surface and a larger particle size of 600 nm. This is due to the wrapping of GA around the Fe_3O_4–NH_2 surface, concealing the small Fe_3O_4–NH_2 particles themselves, thus forming spherical particles with larger particle size and smoother surface.

The FT-IR spectrum of Fe_3O_4–NH_2, GA, and GA@Fe_3O_4–NH_2 were shown in Fig. 2A. In the FT-IR spectra of Fe_3O_4–NH_2, the absorption peak of 586 cm^{-1} was attributed to the vibrations of Fe–O. At the same time, the presence of absorption peaks (attributed to R–NH_2) at 2852 and 2919 cm^{-1} indicated the presence of –NH_2 groups on the magnetic nanoparticles. In contrast to the FT-IR spectrum of Fe_3O_4–NH_2, distinct GA characteristic absorption peaks appeared in the infrared spectrum of GA@Fe_3O_4–NH_2, including $V_{C\text{-}N}$ = 1052 cm^{-1}, $V_{C\text{-}O\text{-}C}$ = 1089 cm^{-1}, γ_{NH} = 881 cm^{-1}. Furthermore, the absorption peak of δ_{NH} changed from 1633 cm^{-1} to 1643 cm^{-1} [33,34]. This was attributed to the formation of hydrogen bonds between the amine functional groups of PEI and the hydroxyl and amino groups of GA, indicating the successful binding of geldanamycin to the surface of the magnetic nanomaterials.

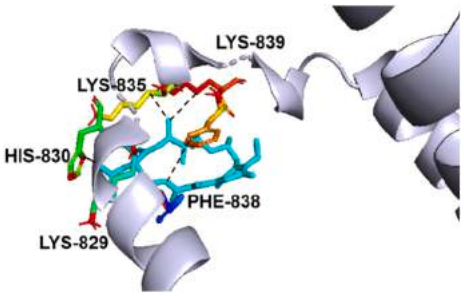

Fig. 3. Molecular dynamics simulation of geldanamycin versus MYO.

The Raman spectra of the Fe_3O_4–NH_2 and GA@Fe_3O_4–NH_2 were shown in Fig. 2B. In the Raman spectrum of Fe_3O_4–NH_2, 215 and 280 cm^{-1} are the characteristic peaks of Fe–O in Fe_3O_4. However, in the Raman spectra of geldanamycin-encapsulated magnetic nanoparticles GA@Fe_3O_4–NH_2, the peaks of Fe–O shifted to large wave number and the relative peak strengths decreased. This is because the Raman signal is generated by the elastic scattering of light on the sample surface, and if the surface was covered, the main peak was from the surface substance [35]. Therefore, 703 and 1399 cm^{-1} were the C–N and C–H characteristic peaks of GA, demonstrating that GA had wrapped around the surface of magnetic nanoparticles.

Fig. 2C is the Energy dispersive X-ray spectrometer (EDS) analysis results of GA@Fe_3O_4–NH_2. The presence of Fe, C, O, and N elements in the product GA@Fe_3O_4–NH_2 further illustrated the successful binding of geldanamycin on the surface of magnetic nanomaterials.

In Fig. 2D, the maximum saturation magnetization value of Fe_3O_4–NH_2 was found to be about 255.43 emu g^{-1}, while the maximum saturation magnetization value of GA@Fe_3O_4–NH_2 for the GA-encapsulated magnetic nanoparticles was about 92.56 emu g^{-1}. This was due to the successful coating of GA attached to the Fe_3O_4–NH_2 surface, resulting in a large decrease in the magnetization value. Nevertheless, GA@Fe_3O_4–NH_2 still maintained good superparamagnetism.

3.2. Protein adsorption properties of the GA@Fe_3O_4–NH_2

To evaluate the affinity of the GA@Fe_3O_4–NH_2 for different proteins, four proteins were selected as model proteins, bovine serum albumin (BSA), myosin (MYO), myoglobin (MYB), and cytochrome C (Cyt-C). Their isoelectric points (pI) are about 4.7, 5.5, 6.9 and 10.1, respectively. The adsorption efficiency of the GA@Fe_3O_4–NH_2 on different proteins within the pH range of 4.0–10.0 was shown in Fig. 4A. At pH 6.0, the adsorption efficiency of MYO reached 97.1 %, while the adsorption efficiency of BSA, MYB and Cyt-C was limited, all lower than 15 %. When the pH value increased, the adsorption efficiency of MYO first increased and then decreased, the adsorption efficiency of MYB gradually decreased, and the adsorption efficiency of Cyt-C slightly increased. For MYO, MYB and Cyt-C, maximum adsorption efficiency was achieved near their isoelectric points. For BSA, the adsorption efficiency was about 15 % in the pH range of 5.0–9.0.

The main forces acting on MYO binding to GA@Fe_3O_4–NH_2 were mainly characterized by hydrophobic and hydrogen bonding interactions. When pH was close to the isoelectric point (pI), the protein had the highest affinity for the carrier due to having no net charge, tending to aggregate, having low solubility and exposing more hydrophobic amino acid residues. Molecular dynamics simulation (Fig. 3) showed that the binding sites were concentrated in the 800–850 amino acid region of the head of myosin. The six key amino acid residues of myosin formed a binding pocket to wrap around the GA molecule. Among them, five amino acid residues-Phe-825 and Phe-838, Lys-829, Lys-835 and Lys-839-bound to three carbon atoms of GA by alkyl

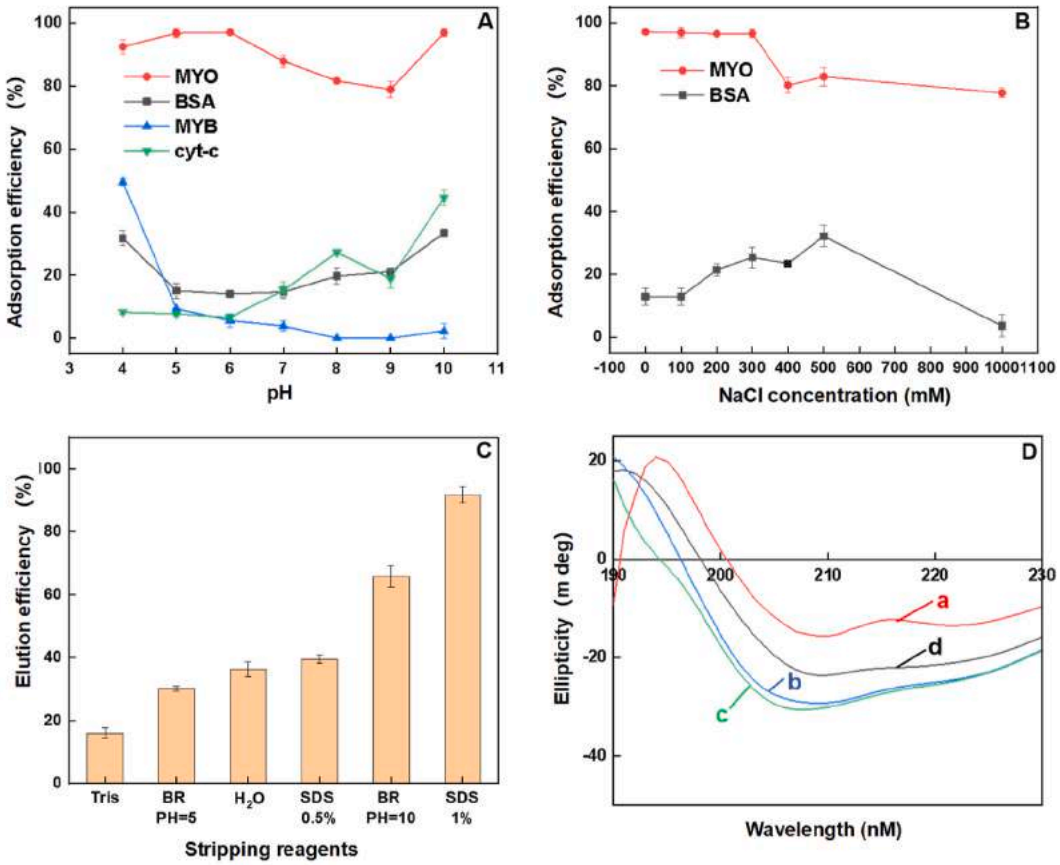

Fig. 4. Effect of pH on adsorption efficiency of MYO, BSA, MYB and Cyt-C onto GA@Fe_3O_4–NH_2 (A). Protein solution:100 μg mL^{-1}, 100 μL; GA@Fe_3O_4–NH_2: 0.1 mg; The effect of the NaCl concentration on the adsorption efficiency of MYO and BSA at pH 6.0 was researched (B). The recoveries of the adsorbed MYO from GA@Fe_3O_4–NH_2 using various buffers as stripping reagents (C). MYO solution: 100 μg mL^{-1}, 100 μL, pH 6.0; GA@Fe_3O_4–NH_2: 0.1 mg; adsorption time: 30 min; stripping reagent volume: 100 μL. Sorbet region CD spectra of MYO (D). 100 μg mL^{-1} MYO in deionized water (a); MYO directly dissolved in SDS solution (1 %, m/m) (b); MYO stripped into SDS solution (1 %, m/m) (c); MYO in the eluate after removal of SDS by use of ultrafiltration with a 10 kDa centrifugal filter (d).

hydrophobic interactions. The imidazole ring of His-830 combined with the carbonyl oxygen atom of GA to form a hydrogen bond. This suggested that this binding pocket was critical for GA targeted recognition and selective adsorption of myosin. In addition, the binding energy of myosin and ligand (−3.25 kJ/mol) was relatively low, indicating the relatively strong binding ability and stability of GA and MYO [36–39]. Therefore, the GA@Fe_3O_4–NH_2 showed good adsorption properties for MYO. At pH 6.0, the GA@Fe_3O_4–NH_2 was significantly higher than BSA, MYB and Cyt-C. Therefore, by controlling the pH value of the solution, selective adsorption of MYO in actual samples can be achieved.

In general, ionic strength has a great influence on the interaction between protein molecules and solid materials. Generally speaking. The effect of NaCl concentration on the adsorption efficiency of MYO and BSA at pH 6.0 was studied, and the experimental results are shown in Fig. 4B. As the concentration of NaCl in the solution increased, the adsorption efficiency of GA@Fe_3O_4–NH_2 on MYO remained stable, both higher than 90 %, while that of BSA gradually decreased. This was due to the presence of salt, which increased the solubility of MYO while increasing the surface tension of the solution, facilitating the exposure of hydrophobic regions inside the protein. Thus, high salt concentrations can promote hydrophobic interactions between protein and GA@Fe_3O_4–NH_2, further improve the adsorption efficiency. Moreover, the salt can inhibit the electrical double layer of proteins, thereby reducing the transverse electrostatic repulsion between adsorbed protein molecules and improving their adsorption efficiency. However, for MYO and BSA, the adsorption efficiency of the proteins gradually decreased when the salt concentration exceeded 300 and 500 mol mL^{-1} respectively. This might have been due to competition between the composition of ionic liquid and the salt ions for being adsorbed on the surface of GA@Fe_3O_4–NH_2. Furthermore, at the maximum concentration of electrolyte, the adsorption efficiency of MYO did not drop sharply, which indicated the existence of hydrophobic and hydrogen bonding interactions.[40,41] Therefore, considering the obtained results and the ubiquitous influence of the salt concentration in the actual samples, ddH_2O was selected as the protein solvent experimentally.

The effect of adsorption temperature of MYO onto GA@Fe_3O_4–NH_2 was investigated. In Fig. 1S (A), 15 °C was selected as the optimal adsorption temperature. The effect of adsorption time on the adsorption efficiency of MYO onto GA@Fe_3O_4–NH_2 was investigated in a range of 10–40 min. As shown in Fig. 1S (B), when the adsorption time was 30 min, the adsorption efficiency of GA@Fe_3O_4–NH_2 on MYO reached the maximum of 97.1 %. In order to investigate the adsorption capacity of GA@Fe_3O_4–NH_2 on MYO, the adsorption capacities at different concentrations of MYO (100–700 μg mL^{-1}) were investigated. The results of the adsorption capacity of GA@Fe_3O_4–NH_2 for MYO at different concentrations were shown in Fig. 1S (C). As shown in Fig. 1S (D), there was a linear relationship between $1/q_{eq}$ and $1/C_e$. The linear equation was $1/q_{eq} = 0.01229C_e + 0.00193$, and the correlation coefficient $R^2 = 0.98809$. According to the intercept calculation of the straight line in Fig. 1S (D), the theoretical maximum adsorption capacity Q_m was 518.1 mg g^{-1}.

In actuality, it was important to elute the adsorbed proteins from the adsorbent into a suitable aqueous medium to facilitate further biological research. Different solutions had been used for stripping of the adsorbed MYO from GA@Fe_3O_4–NH_2, for example, Tris (100 mmol L^{-1}), BR buffer (pH 5.0, 0.04 mol L^{-1}), ddH_2O, SDS solution (0.5 %, m/m), BR

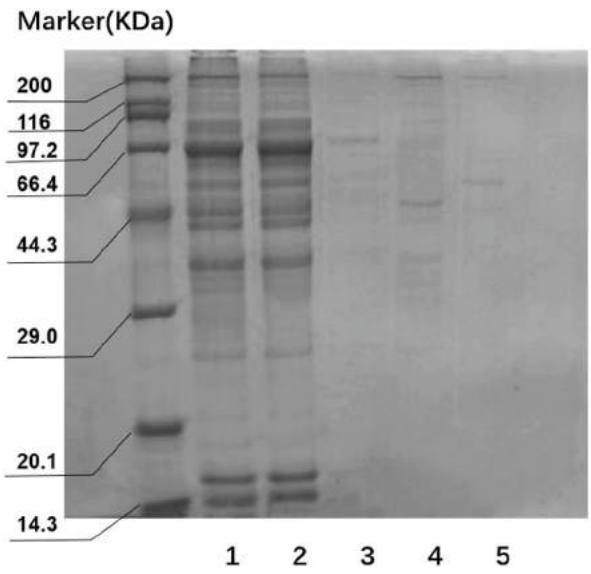

Fig. 5. SDS-PAGE assay results. Lane 1: pig heart protein extract; Lane 2: pig heart protein extract after adsorption with GA@Fe_3O_4–NH_2 as adsorbent; Lane 3: The supernatant after washing the GA@Fe_3O_4–NH_2 adsorbing myosin with BR buffer (pH 6.0, 0.04 mol L^{-1}); Lane 4: the collected myosin by stripping with SDS solution (1 %, m/m); Lane 5: 100 μg mL^{-1} MYO solution.

buffer (pH 10.0, 0.04 mol L^{-1}) and SDS solution (1 %, m/m). As shown in Fig. 4C, the maximum elution efficiency of MYO was 91.8 % by using 1 % SDS solution as eluent.

To evaluate whether myosin eluted from GA@Fe_3O_4–NH_2 with SDS solution (1 %, m/m) as the eluent was denatured, far-UV circular dichroism (CD) spectra were used to study the conformational changes of MYO (Fig. 4D). Fig. 4D (a) was a CD spectrum of myosin dissolved in ddH_2O, with two negative peaks at 210 nm and 222 nm, attributed to the α helical structure of the protein. After elution of myosin with SDS solution (1 %, m/m), the peaks changed to 208 nm and 220 nm (Fig. 4D (c)), indicating a change in myosin conformation. The reason for the conformational change was the existence of two possibilities: it could have been caused by GA@Fe_3O_4–NH_2 during the adsorption of myosin or by the eluting agent SDS itself. In order to determine the cause of the conformational change in myosin, myosin was dissolved in SDS solution (1 %, m/m), and the CD spectrum of the solution was determined (Fig. 4D (c)). The peak was consistent with the elution of myosin, indicating that it was most likely caused by SDS solution. In order to determine whether the conformational change was reversible, the resulting myosin eluate was desalted using a 10 kDa ultrafiltration tube, and ddH_2O was added to measure the CD spectrum of myosin (Fig. 4D (d)), which was consistent with the circular dichroism spectrum of myosin in ddH_2O. This result demonstrated that GA@Fe_3O_4–NH_2 had excellent biocompatibility and that the changes in myosin conformation were reversible in the process of adsorption and elution.

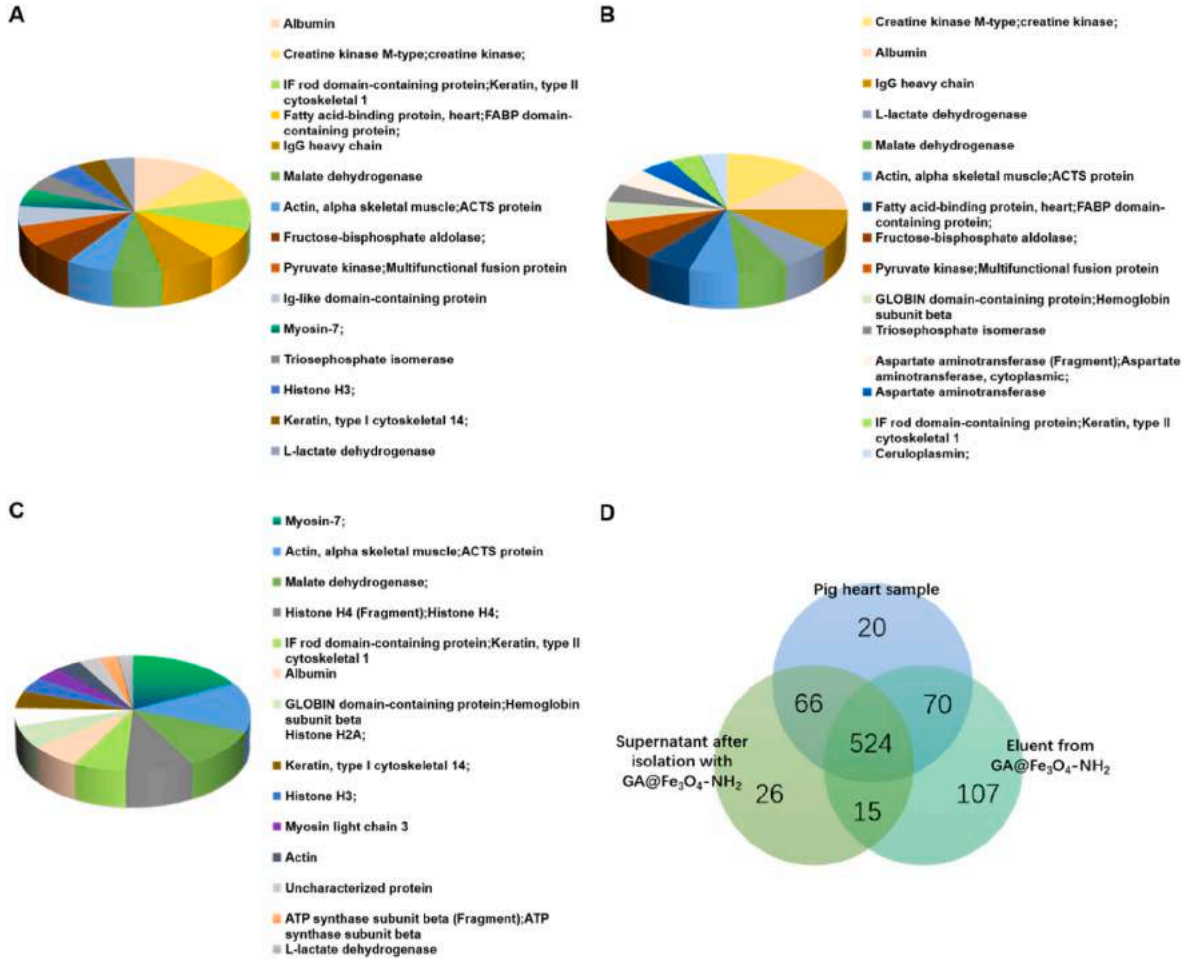

Fig. 6. Mass spectrometry data. Distribution of the top 15 most high-abundance proteins in pig heart (A); The supernatant after isolation of MYO by GA@Fe_3O_4–NH_2 (B); The elution with SDS solution (1 %, m/m) (C); Venn diagram of protein species distribution in the pig heart, supernatant adsorbed by GA@Fe_3O_4–NH_2 and eluent recovered from the surface of GA@Fe_3O_4–NH_2 (D).

3.3. Isolation and purification of MYO from pig heart extract by GA@Fe_3O_4–NH_2

The results of SDS-PAGE of myosin in purified pig heart extract were shown in Fig. 5. In Lane 1, a protein extract from the left ventricle of the pig heart, showed hundreds of protein bands in the range of 10–200 kDa, of which 200 kDa was myosin. Lane 2 was the supernatant after the pig heart protein extract was adsorbed by GA@Fe_3O_4–NH_2, apparently showing the 200 kDa band becoming shallower. Lane 3 was the band after pre-washing with BR buffer to remove some of the non-specifically adsorbed proteins. Lane 4 was the supernatant recycled after elution with SDS solution (1 %, m/m), with one protein band appearing at 200 kDa, consistent with MYO band. The other band was 44 kDa, attributed to actin. This was due to the fact that myosin head segment can bind a large amount of actin.[42] Therefore, when GA@Fe_3O_4–NH_2 sspecifically adsorbed myosin, it also carried a certain amount of actin. This well suggested a high purity for the recovered MYO.

To evaluate the utility of GA@Fe_3O_4–NH_2 in proteomics, 1 mL of pig heart protein samples was compared with 1.0 mg GA@Fe_3O_4–NH_2 for the solid-phase extraction process described previously. Fig. 6 showed the analysis of mass spectrometry data during the processing of pig heart samples by GA@Fe_3O_4–NH_2. Results from the LC-MS analysis showed that the pig heart samples themselves contained a higher content of myosin, which decreased significantly after GA@Fe_3O_4–NH_2 treatment. In the supernatant treated with SDS solution (1 %, m/m), MYO had the highest peak intensity and score, which proved the highest amount of MYO purified (Fig. 6C). The above results showed that MYO in the pig heart sample was successfully separated by GA@Fe_3O_4–NH_2. As can be clearly seen in Fig. 6C, GA@Fe_3O_4–NH_2 adsorbed myosin in the pig heart, while a large amount of actin was also isolated. As mentioned above, this was due to the combination of actin and myosin head segment in muscle, while GA had specific adsorption to MYO, resulting in actin adsorption together with MYO. From Figs. 6D and 107 new proteins were identified after treating the pig heart samples with GA@Fe_3O_4–NH_2, which indicated that GA@Fe_3O_4–NH_2 successfully removed high-abundance proteins from the pig heart samples, thus identifying some low-abundance proteins. Therefore, using this method, we could identify a total of 716 proteins, while the untreated pig heart samples identified only 680 proteins, indicating the potential application value of GA@Fe_3O_4–NH_2 in proteomics.

4. Conclusions

In this study, geldanamycin-encapsulated magnetic nanoparticles (GA@Fe_3O_4–NH_2) were successfully synthesized and characterized by FT-IR, Raman, SEM, EDS, VSM and TEM. Due to the high affinity between GA and myosin, the composite exhibited excellent biocompatibility and high selectivity for myosin. Therefore, in practice, the constructed GA@Fe_3O_4–NH_2 was used for the isolation and purification of myosin from pig heart. The effectiveness of this method will lay a foundation for the research of proteomics. The separation and purification of myosin can help further study the pathogenesis and preventive measures of cardiac diseases such as ventricular dysfunction, heart failure and arrhythmia, thereby effectively treating heart diseases. In conclusion, drug-based MNPs hold immense promise in proteomic studies, offering novel approaches for protein isolation, protein-protein interaction analysis, biomarker discovery. These applications have the potential to revolutionize proteomics research and contribute to advancements in diagnostics, therapeutics, and personalized medicine.

Credit author statement

Qing Chen: Validation, Writing-review and editing, Funding acquisition, Project administration. Yan Xu: Writing-review and editing, Software, Investigation. Xue Ting Feng: Methodology, Investigation. Yuhan Xiang: Investigation. Jiayue Ni: Investigation. Guo-yu Ding: Supervision, Investigation, Writing-original draft, Qunxiang Ren: Conceptualization, Methodology, Investigation, Project administration, Funding acquisition. Ming-sheng Zhou: Investigation, Funding acquisition.

Declaration of competing interest

The authors declare that they have no known competing financial interests or personal relationships that could have appeared to influence the work reported in this paper.

Data availability

No data was used for the research described in the article.

Acknowledgments

The authors appreciate financial support from the National Natural Science Foundation of China (21804093, 82270434 and 81970357), the Natural Science Foundation of Liaoning Province (2023-MS-324 and 2023JH/10300079) and Student Research Project of Shenyang Medical College (20229005).

Appendix A. Supplementary data

Supplementary data to this article can be found online at https://doi.org/10.1016/j.talanta.2023.125294.

References

[1] S. Zhuang, Y. Liu, S. Gao, Y. Tan, H. Hong, Y. Luo, Mechanisms of fish protein degradation caused by grass carp spoilage bacteria: a bottom-up exploration from the molecular level, muscle microstructure level, to related quality changes, Food Chem. 403 (2023), 134309.
[2] L.K. Fuerniss, B.J. Johnson, Semi-automated technique for bovine skeletal muscle fiber cross-sectional area and myosin heavy chain determination, J. Anim. Sci. 101 (2023) 205.
[3] R.F. Kawas, R.L. Anderson, S.R.B. Ingle, Y. Song, A.S. Sran, H.M. Rodriguez, A small-molecule modulator of cardiac myosin acts on multiple stages of the myosin chemomechanical cycle, J. Biol. Chem. 292 (2017) 16571–16577.
[4] B.J. Foth, M.C. Goedecke, D. Soldati, New insights into myosin evolution and classification, PANS (Pest. Artic. News Summ.) 103 (2006) 3681–3686.
[5] M. Krendel, M.S. Mooseker, Myosins: tails (and heads) of functional diversity, Physiology 20 (2005) 239–251.
[6] G. Kessler-Icekson, Effect of triiodothyronine on cultured neonatal rat heart cells: beating rate, myosin subunits and CK-isozymes, J. Mol. Cell. Cardiol. 20 (1988) 649–655.
[7] N. Shalitin, M. Friedman, H. Schlesinger, The effect of angiotensin II on myosin heavy chain expression in cultured myocardial cells, in Vitro Cell, Dev. Biol.-Animal 32 (1996) 573–578.
[8] S. Liu, Z. Li, B. Yu, S. Wang, Y. Shen, H. Con, Recent advances on protein separation and purification methods, Adv. Colloid and Interfac. 284 (2020), 102254.
[9] S. Büyüktiryaki, R. Keçili, C.M. Hussain, Functionalized nanomaterials in dispersive solid phase extraction: advances & prospects, TrAC, Trends Anal. Chem. 127 (2020), 115893.
[10] A. Gentili, Cyclodextrin-based sorbents for solid phase extraction, J. Chroma. A 1609 (2020), 460654.
[11] X. Hai, M. Ji, K. Yu, T. Tian, Z. Cui, S. Bi, X. Zhang, Acid-responsive DNA-Au nanomachine with active/passive dual-targeting capacity for combinational cancer therapy, Materials Today Nano 23 (2023), 100355.
[12] X.W. Chen, S. Chen, J.H. Wang, A pH-responsive poly(N-isopropylacrylamide-co-acrylic acid) hydrogel for the selective isolation of hemoglobin from human blood, Analyst 135 (2010) 1736–1741.
[13] X. Zhang, X. Zhu, Y. Li, X. Hai, S. Bi, A colorimetric and photothermal dual-mode biosensing platform based on nanozyme-functionalized flower-like DNA structures for tumor-derived exosome detection, Talanta 258 (2023), 124456.
[14] M.L. Chen, M. Li Chen, X.W. Chen, J.H. Wang, Functionalization of MWNTs with hyperbranched PEI for highly selective isolation of BSA, Macromol. Biosci. 10 (2010) 906–915.
[15] S. Tang, W. Wan, X.W. Chen, J.H. Wang, Fluoridized iron phosphate as a novel adsorbent for selective separation/isolation of cytochrome c, Anal. Bioanal. Chem. 401 (2011) 3283–3292.
[16] X. Zhu, T. Li, X. Hai, S. Bi, A nanozyme-based colorimetric sensor array as electronic tongue for thiols discrimination and disease identification, Biosens. Bioelectron. 213 (2022), 114428.

[17] R. Karami-Osboo, F. Ahmadpoor, M. Nasrollahzadeh, M. Maham, Polydopamine-coated magnetic Spirulina nanocomposite for efficient magnetic dispersive solid-phase extraction of aflatoxins in pistachio, Food Chem. 377 (2022), 131967.
[18] Y. Pan, X. Du, F. Zhao, Magnetic nanoparticles for the manipulation of proteins and cells, Chem. Soc. Rev. 41 (2012) 2912–2942.
[19] Y. Li, X. Zhang, C. Deng, Functionalized magnetic nanoparticles for sample preparation in proteomics and peptidomics analysis, Chem. Soc. Rev. 42 (2013) 8517–8539.
[20] C.L. Altan, B. Gurten, R. Sadza, E. Yenigul, N.A.J.M. Sommerdijk, S. Bucak, Poly (acrylic acid)-directed synthesis of colloidally stable single domain magnetite nanoparticles via partial oxidation, J. Magn. Magn Mater. 416 (2016) 366–372.
[21] R. Minkner, J. Xu, K. Takemura, J. Boonyakida, H. Wätzig, E.Y. Park, Ni-modified magnetic nanoparticles for affinity purification of His-tagged proteins from the complex matrix of the silkworm fat body, J. Nanobiotechnol. 18 (2020) 159.
[22] H.M. Lee, H.G. Kang, Rapid and simultaneous purification of aflatoxin B1, zearalenone and deoxynivalenol using their monoclonal antibodies and magnetic nanoparticles, Toxicol. Res. (2021) 1–7.
[23] J. Hermane, S. Eichner, L. Mancuso, B. Schröder, F. Sasse, C. Zeilinger, A. Kirschning, New geldanamycin derivatives with anti Hsp properties by mutasynthesis, Org. Biomol. Chem. 17 (2019) 5269–5278.
[24] K. Ojima, E. Ichimura, T. Suzuki, M. Oe, S. Muroya, T. Nishimura, HSP90 modulates the myosin replacement rate in myofibrils, Am. J. Physiol.-Cell Ph. 315 (2018) 104–114.
[25] S. Suttitanamongkol, A.R. Gear, Polanowska-Grabowska R. Geldanamycin, Disrupts platelet-membrane structure leading to membrane permeabilization and inhibition of platelet aggregation, Biochem. J. 345 (2000) 307–314.
[26] Y. Fukuyo, C.R. Hunt, N. Horikoshi, Geldanamycin and its anti-cancer activities, Cancer Lett. 290 (2010) 24–35.
[27] S.G. Sun, M.H. Ma, N. Qiu, Affinity adsorption and separation behaviors of avidin on biofunctional magneticnanoparticles binding to iminobiotin, Colloids Surf. B Biointerfaces 88 (2011) 246–253.
[28] W. Ma, S. Xu, J. Li, J. Guo, Y. Lin, C. Wang, Hydrophilic dual-responsive magnetite/PMAA core/shell microspheres with high magnetic susceptibility and pH sensitivity via distillationprecipitation polymerization, Polym. Sci., Part A: Polym. Chem. 49 (2011) 2725–2733.
[29] M. Nonaka, H. Mabashi-Asazuma, D.L. Jarvis, Development of an orally-administrable tumor vasculature-targeting therapeutic using annexin A1-binding D-peptides, PLoS One 16 (2021), 0241157.
[30] Y. Pan, Z. Wang, S. Xu, L. Zhang, W. Zhang, Selective profiling of liver-related specific proteins based on sofosbuvir-modified magnetic separation material, Anal. Sci. 39 (2023) 313–323.
[31] B. Yilmaz, O. Ozay, Synthesis of antibiotic-modified silica nanoparticles and their use as a controlled drug release system with antibacterial properties, Phosphorus, Sulfur, and Silicon and the Related Elements 197 (2022) 964–972.
[32] F. Zhang, H. Cao, D. Yue, Z. Zhou, Graphene covalently modified by DNA G-base, J. Phys. Chem. C 117 (2013) 3513–3519.
[33] M.S. Islam, W.S. Choi, H.J. Lee, Controlled etching of internal and external structures of SiO_2 nanoparticles using hydrogen bond of polyelectrolytes, ACS Appl. Mater. Interfaces 6 (2014) 9563–9571.
[34] S. Ashtiani, M. Khoshnamvand, D. Bouša, J. Šturala, Z. Sofer, A. Shaliutina-Kolešová, D. Gardenö, K. Friess, Surface and interface engineering in CO_2-philic based UiO-66-NH_2-PEI mixed matrix membranes via covalently bridging PVP for effective hydrogen purification, Int. J. Hydrogen Energy 46 (2021) 5449–5458.
[35] Q. Chen, X. Hu, D.D. Zhang, X.W. Chen, J.H. Wang, Selective isolation of myosin Subfragment-1 with a DNA-Polyoxovanadate bioconjugate, Bioconjugate Chem. 28 (2017) 2976–2984.
[36] L. Wei, L. Cao, S. Xiong, Y. Hu, R. Liu, Effects of pH on self-assembly of silver carp myosin at low temperature, Food Biosci. 30 (2019), 100420.
[37] H. Liu, X. Wei, R. Nie, Molecular docking simulation combining with multi-spectroscopy techniques clarify how small molecule ligands bind to biomacromolecule: myosin and aldehydes as a case study, LWT 155 (2022), 112977.
[38] X. Chen, Y. Zou, M. Han, L. Pan, T. Xing, X. Xu, G. Zhou, Solubilisation of myosin in a solution of low ionic strength L-histidine: significance of the imidazole ring, Food Chem. 196 (2016) 42–49.
[39] C. Xue, J. You, S. Xiong, Myosin head as the main off-odors binding region: key binding residues and conformational changes in the binding process, Food Chem. 403 (2023), 134437.
[40] S. Kamran, M. Asadi, G. Absalan, Adsorption of acidic, basic, and neutral proteins from aqueous samples using Fe_3O_4 magnetic nanoparticles modified with an ionic liquid, Microchim. Acta 180 (2013) 41–48.
[41] M.M.H. Antink, S. Beutel, K. Rezwan, Tailoring electrostatic surface potential and adsorption capacity of porous ceramics by silica-assisted sintering, Materialia 12 (2020), 100735.
[42] T.J. Stewart, V. Murthy, S.P. Dugan, J.E. Baker, Velocity of myosin-based actin sliding depends on attachment and detachment kinetics and reaches a maximum when myosin-binding sites on actin saturate, J. Bio. Chem. 297 (2021), 101178.